Semicond. Sci. Technol. **31** (2016) 095003 (8pp) doi:10.1088/0268-1242/31/9/095003

Responsivity drop due to conductance modulation in GaN metal-semiconductor-metal Schottky based UV photodetectors on Si(111)

L Ravikiran[1], K Radhakrishnan[1], N Dharmarasu[2], M Agrawal[2], Zilong Wang[3], Annalisa Bruno[4], Cesare Soci[3,5], Tng Lihuang[2] and Ang Kian Siong[2]

[1] Centre for Micro-/Nano-electronics (NOVITAS), School of Electrical and Electronic Engineering, Nanyang Technological University, 50 Nanyang Drive, Singapore 639798
[2] Temasek Laboratories@NTU, Nanyang Technological University, 50 Nanyang Drive, Singapore 637553
[3] Division of Physics and Applied Physics, School of Physical and Mathematical Sciences, Nanyang Technological University, 21 Nanyang Link, Singapore 637371
[4] Singapore-Berkeley Research Initiative for Sustainable Energy, Energy Research Institute @ NTU (ERI@N), Research Techno Plaza, Nanyang Technological University, 50 Nanyang Drive, Singapore 637553
[5] Centre for Disruptive Photonic Technologies, Nanyang Technological University, Nanyang, 21 Nanyang Link, Singapore 637371

E-mail: ERADHA@e.ntu.edu.sg

Received 4 April 2016, revised 7 June 2016
Accepted for publication 28 June 2016
Published 28 July 2016

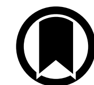

Abstract

GaN Schottky metal-semiconductor-metal (MSM) UV photodetectors were fabricated on a 600 nm thick GaN layer, grown on 100 mm Si (111) substrate using an ammonia-MBE growth technique. In this report, the effect of device dimensions, applied bias and input power on the linearity of the GaN Schottky-based MSM photodetectors on Si substrate were investigated. Devices with larger interdigitated spacing, '*S*' of 9.0 μm between the fingers resulted in good linearity and flat responsivity characteristics as a function of input power with an external quantum efficiency (*EQE*) of ~33% at an applied bias of 15 V and an input power of 0.8 W m^{-2}. With the decrease of '*S*' to 3.0 μm, the *EQE* was found to increase to ~97%. However, devices showed non linearity and drop in responsivity from flatness at higher input power. Moreover, the position of dropping from flatter responsivity was found to shift to lower powers with increased bias. The drop in the responsivity was attributed to the modulation of conductance in the MSM due to the trapping of electrons at the dislocations, resulting in the formation of depletion regions around them. In devices with lower '*S*', both the image force reduction and the enhanced collection efficiency increased the photocurrent as well as the charging of the dislocations. This resulted in the increased depletion regions around the dislocations leading to the modulation of conductance and non-linearity.

Keywords: GaN on Si, GaN UV detector, MSM devices, non-linearity, ammonia-MBE, responsivity drop

(Some figures may appear in colour only in the online journal)

 © 2016 IOP Publishing Ltd Printed in the UK

1. Introduction

The increased demand for ultraviolet (UV) photodetectors from civil, industrial, military and space sectors necessitates their development with improved performance at cheaper cost. GaN-based alloys are one of the key material systems for the development of UV photodetectors because of their wide bandgap, high electron saturation velocity and high breakdown field strength that allow high temperature, high frequency and high power operations [1]. Moreover, the high chemical and radiative hardness of GaN-based alloys permit the operation of these devices in challenging environments [2]. Ever since the first report of a GaN-based photoconductor by Khan *et al* [3], GaN-based photodetectors have been intensely studied and different kinds of photodetector device structures such as photoconductors [3, 4], Schottky based photodetectors [4–6], p-n junction devices [7, 8], p-i-n junction devices [9, 10] and metal-semiconductor-metal (MSM) [11, 12] photodetectors were investigated. Among these different structures, MSM photodetectors have advantages such as ease of fabrication due to planar technology, large active area, small capacitance and fast response characteristics [13]. However, MSM devices were found to result in an intrinsic gain, which leads to the increase of the responsivity as a function of applied bias and input power. The gain in these devices has been majorly attributed to two different phenomena, and they are, barrier lowering due to image force reduction [14] and trapping of charge carriers at the metal semiconductor interface [15, 16]. In contrast, Monroy *et al* have observed a drop in the responsivity as a function of input power for GaN-based photo conductors [4]. But a flat responsivity characteristic was observed for Schottky-based photodetectors fabricated on the same material. Based on the modelling by Garrido *et al* [17], they have attributed the drop in the responsivity in the photoconductor to modulation of conductance due to the trapping of electrons in the dislocations. However, to the best of our knowledge, either such behaviour of a drop in responsivity characteristics or its dependence on applied bias, device dimensions and input power have not been reported for GaN Schottky MSM devices. Hence, in this report, we have investigated both the flat and drop in the responsivity regions of a Schottky- based GaN MSM photodetector grown on Si substrate by ammonia-MBE by varying the applied bias, device dimensions and input power.

2. Experimental

The epilayer structure of GaN-based photodetector on 100 mm Si (111) grown using ammonia-MBE is shown in figure 1(a). The nucleation process of AlN on Si involves intentional nitridation of the Si surface to achieve crystalline Si_3N_4 formation followed by the pre-deposition of few monolayers of aluminium and subsequent ramp-up to AlN growth temperature. Following the nucleation process, AlN and GaN epilayers were grown at growth temperatures of 920 and 800 °C, respectively. The epilayer structure of a GaN-based photodetector on 100 mm Si (111) grown using ammonia-MBE is shown in figure 1(a). Unlike the epilayer structure for high electron mobility transistors grown using ammonia-MBE on Si substrate, where thick GaN buffer layers and the use of AlN/GaN [18, 19] or AlGaN/AlN/GaN [20] stress mitigating layers (SMLs) were necessary, the epilayer structure for photodetector application in this study was designed using simple AlN and GaN epilayers with thicknesses of 200 and 600 nm, respectively. Their corresponding growth rates were kept constant at 0.13 and 0.70 $\mu m\ h^{-1}$, respectively. The complete details on the nucleation and growth of GaN and AlN epilayers on Si by ammonia-MBE can be found elsewhere [21]. The simple epilayer structure of a photodetector not only reduces the usage of resources but also increases the throughput of epiwafer growth. Surface morphology of grown epilayers was studied using an optical microscope, operated in differential interference contrast (DIC) mode and also using an atomic force microscope (AFM). While structural properties of epilayers were studied using a high resolution x-ray diffraction (HR-XRD) technique, optical properties were studied using room temperature photoluminescence (RT-PL) and micro-Raman spectroscopy.

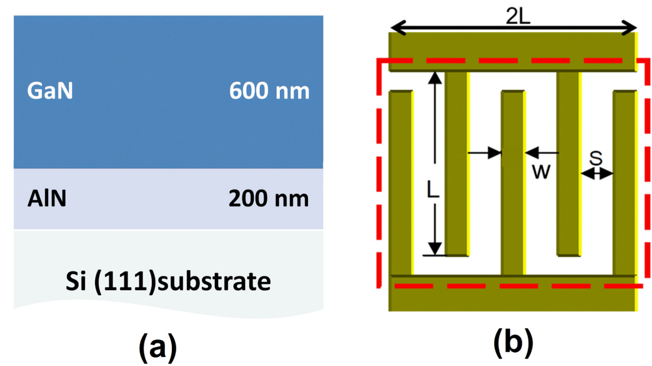

Figure 1. (a) Epilayer structure of a GaN-based photodetector on Si substrate, (b) the schematic of the MSM photodetector.

Metal-semiconductor-metal (MSM) interdigitated structures were fabricated on GaN with Ni/Au contacts of thicknesses 150/350 nm. A schematic picture of the MSM structure is shown in figure 1(b). Three different MSM structures were investigated in this study, namely D1, D2 and D3. The interdigitated finger width (*W*) and spacing (*S*) in μm of D1, D2 and D3 were varied as W6.5S9.0, W4.5S4.5 and W3.0S3.0, respectively. In all these MSM structures, the finger-length (*L*) was kept at 250 μm, and the fingers were connected by two contact pads with a length and width of 500 and 100 μm, respectively. Current–voltage characteristics of the devices in the dark and under illumination were measured using a Keithley-6478 picoammeter and a voltage source in the DC measurement mode. The photodetector spectral responsivity characteristics were studied with an amplitude modulation technique. The monochromatic light was generated by a combination of Xenon lamp source and JY-IHR 550 monchromator, and modulated by a mechanical chopper at a frequency of 130 Hz. The photocurrent was detected by a

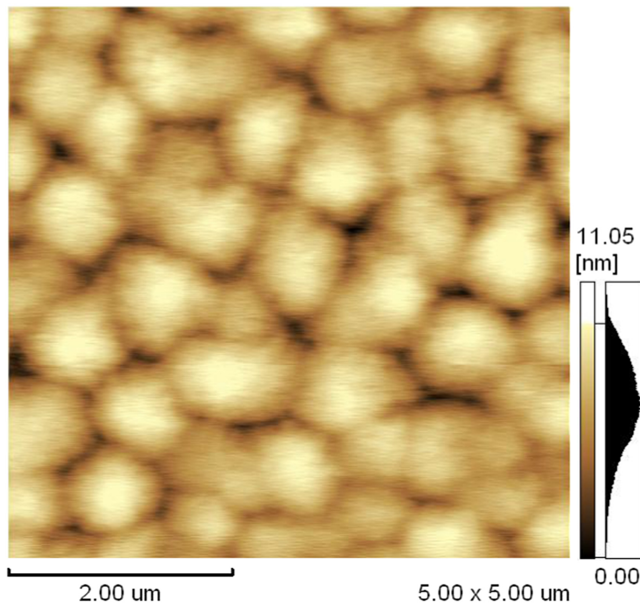

Figure 2. AFM surface morphology over a 5 × 5 μm^2 scanned area of a GaN epilayer structure.

lock-in amplifier (SR 830) [22]. The optical power density of the incident light was varied using a set of neutral filters and was calibrated using a UV-enhanced Si photodiode.

3. Results and discussion

A microscopic investigation of the grown epilayers showed no surface or buried cracks in the epilayer structure. This indicates that the GaN layer has sufficient residual compression at the end of the growth, which compensates the tensile stress generated during the cool-down resulting in a crack-free wafer. The atomic force microscopy (AFM) investigation of the surface revealed a mound type surface morphology [23] as shown in figure 2, which is a characteristic feature of ammonia-MBE growth. The root mean square (RMS) surface roughness measured was ~2 nm for a scan area of 5 × 5 μm^2.

The crystal quality of the GaN epilayer was studied using HR-XRD (high resolution x-ray diffraction) rocking curve scans along (0002) and $(30\bar{3}2)$ planes of GaN, whose full width at half maxima (FWHM) were 900 and 2919 arc-sec, respectively. The FWHM of the rocking curves along GaN (0002) and $(30\bar{3}2)$ represent screw and edge components of dislocation densities, respectively. While the FWHM of rocking curve along GaN (0002) is comparable to that of thick GaN buffer layers grown using AlN/GaN SMLs [24], the FWHM of rocking curve along the GaN $(30\bar{3}2)$ plane is found to be relatively higher. A lower thickness of GaN and lack of multiple interfaces in this structure lead to relatively lesser annihilation of edge-type dislocations by dislocation bending and looping mechanisms [25]. Nevertheless, a simple epilayer device structure with a thinner GaN layer helps to achieve higher throughput and lower cost.

Figure 3 shows the photoluminescence (PL) spectra obtained at room temperature (RT) using a He-Cd laser

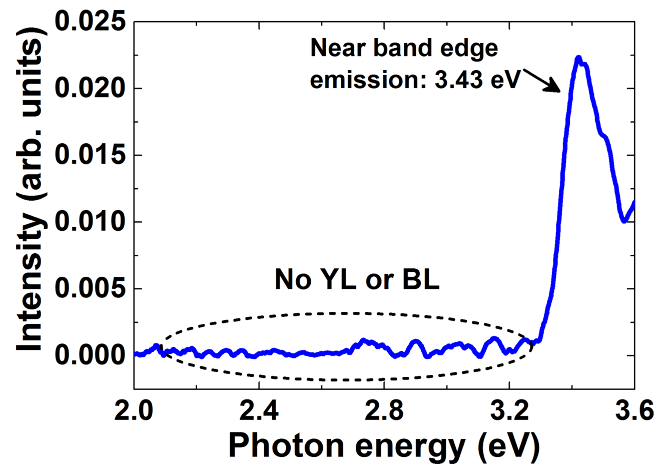

Figure 3. PL spectrum of a GaN epilayer obtained at room temperature.

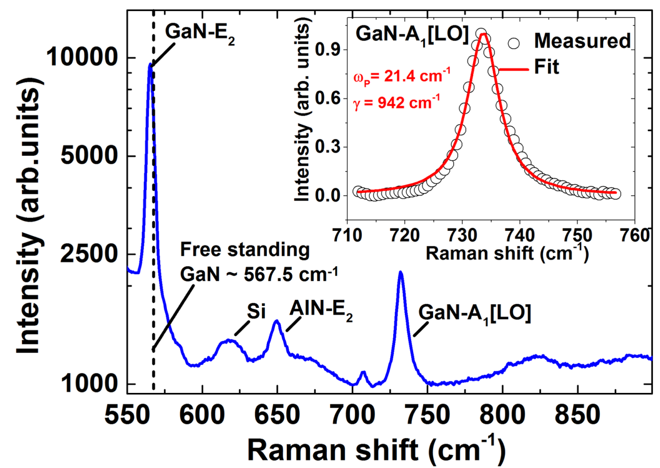

Figure 4. Raman spectrum of the epilayer structure of a photodetector obtained in back scattering geometry. The inset shows A1 [LO] mode with line shape fitting.

source with excitation energy of 3.81 eV. The PL spectrum shows near band-edge luminescence at 3.43 eV with no signal from either the yellow luminescence (YL) (~2.2 eV) or blue luminescence (BL) (~2.9 eV) [26]. The absence of YL and BL suggests that the corresponding defect states are at a minimal level in these samples, indicating the good quality of the GaN epilayer.

A typical Raman spectrum of the sample is shown in the figure 4. It consists of peaks corresponding to GaN-E_2, GaN-A_1 [LO] and AlN-E_2 phonon modes in addition to peaks corresponding to Si. The GaN-E_2 phonon peak position was observed at 565.5 cm^{-1}, which is red-shifted with respect to the free standing GaN-E_2 peak positon of 567.5 cm^{-1}. This indicates the tensile nature of the epilayer with a tensile stress of ~465 MPa, estimated using the relation between biaxial stress and Raman shift of $\Delta\omega = 4.3\ cm^{-1}\ GPa^{-1}$ [27]. Thus, by considering a thermal mismatch tensile stress of ~1.04 GPa between GaN and Si that develops during wafer cool down from growth temperature to room temperature, one can estimate a residual compressive stress of 577 MPa in GaN

at the end of its growth. Hence, this compressive stress partly compensated the thermal mismatch stress and resulted in a crack-free wafer.

The high resistive nature of GaN makes it difficult to form ohmic contacts and measure carrier concentration and mobility by Hall measurements. Hence, to determine the carrier concentration in GaN, the line-shape analysis [28, 29] of A_1 [LO] phonon mode (equation (1)), derived based on a semi classical model involving the deformation potential and electro-optical mechanism was adopted.

$$I(\omega) = KA(\omega)\, Im \times \left[\frac{-1}{\in(\infty)\left[1 + \frac{\omega_L^2 - \omega_T^2}{\omega_L^2 - \omega^2 - i\omega\Gamma} - \frac{\omega_p^2}{\omega(\omega + i\gamma)}\right]}\right], \quad (1)$$

Here, K is the proportionality factor and $A(\omega)$ is given by,

$$A(\omega) = 1 + \frac{2C\omega_T^2[\omega_p^2\gamma(\omega_T^2 - \omega^2) - \omega^2\Gamma(\omega^2 + \gamma^2 - \omega_p^2)]}{\Delta} + C^2\left(\frac{\omega_T^4}{\Delta(\omega_L^2 - \omega_T^2)}\right)\{\omega_p^2[\gamma(\omega_L^2 - \omega_T^2) + \Gamma(\omega_P^2 - 2\omega^2)] + \omega^2\Gamma(\omega_P^2 + \gamma^2)\} \quad (2)$$

where, Δ is given by

$$\Delta = \omega_p^2\gamma[(\omega_T^2 - \omega^2)^2 + (\omega\Gamma)^2] + \omega^2\Gamma(\omega_L^2 - \omega_T^2)(\omega^2 + \gamma^2) \quad (3)$$

$$\omega_P = \sqrt{\frac{4\pi n e^2}{m^*\epsilon\epsilon_0}} \quad (4)$$

$$\gamma = \frac{e}{m^*\mu} \quad (5)$$

Here, ω_L and ω_T are the frequencies of longitudinal optical and transverse optical phonon modes, respectively. Further, n, γ, Γ and ω_P are the carrier concentration, plasmon damping constant, phonon damping constant and plasmon frequency, respectively. For fitting equation (1) to the measured GaN-A1 [LO] modes, frequencies of $\omega_L = 533\ \text{cm}^{-1}$ and $\omega_T = 733.6\ \text{cm}^{-1}$ were considered. Instead of taking a standard value of $734\ \text{cm}^{-1}$ [30] for ω_T, its value was experimentally obtained from Raman measurements on high resistive GaN wafers, where shift due to plasmon–phonon interaction is minimal [31]. The Faust–Henry coefficient, $C = 0.48$ and the GaN constants, $\in(\infty) = 5.35$ and $m^* = 0.2m_0$ were adopted [32]. The inset of figure 6 shows the measured and the line shape fitting of equation (1), which resulted in ω_P and γ of 21.4 and $942\ \text{cm}^{-1}$, respectively. The corresponding carrier concentration and mobility estimated from equations (4) and (5) were $5.46 \times 10^{15}\ \text{cm}^{-3}$ and $49.5\ \text{cm}^2\ \text{V}^{-1}.\text{s}^{-1}$, respectively.

Dark current measurements obtained in the DC measurement mode on MSM devices D1, D2 and D3 resulted in non-linear symmetrical curves [33] as shown in figure 5,

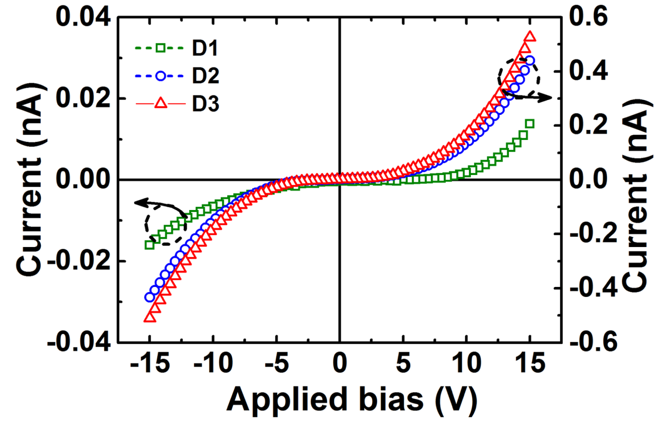

Figure 5. Dark current measurements obtained in the DC measurement mode on MSM devices D1, D2 and D3.

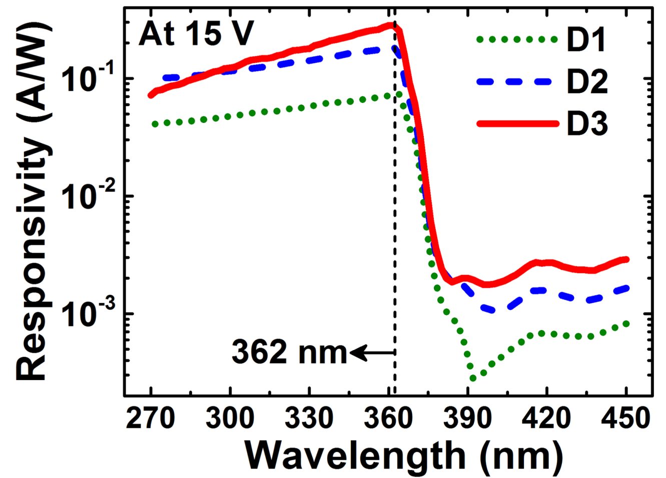

Figure 6. Responsivity of MSM devices D1, D2 and D3 as a function of incident wavelength at the applied bias of 15 V.

with dark current values of 0.016, 0.430 and 0.510 nA, respectively at an applied bias of 15 V. N-rich growth conditions of ammonia-MBE [34], lower intrinsic carrier concentration as estimated from Raman A_1[LO] analysis and the presence of relatively lower screw-type dislocation density can be attributed to the lower dark current in these devices.

Figure 6 shows the photo responsivity ($R = \frac{I_{ph}}{P_{in}}$, where I_{ph} and P_{in} are the photocurrent and power of incident light, respectively) characteristics of D1, D2 and D3 as a function of wavelength of the incident light at an applied bias of 15 V. As shown in this figure, the peak of the spectral responsivity is observed at 362 nm with sharp cut-off in the visible region. The peak responsivities of devices D1, D2 and D3 are 0.0732, 0.183 and $0.282\ \text{A W}^{-1}$, respectively, which correspond to the external quantum efficiencies ($EQE = R\left(\frac{hc}{\lambda}\right)$ where h, c and λ are Planks constants, velocity of light and wavelength of incident light, respectively) of 25.09, 68.89 and 96.71%, respectively. Moreover, an UV/visible rejection ratio

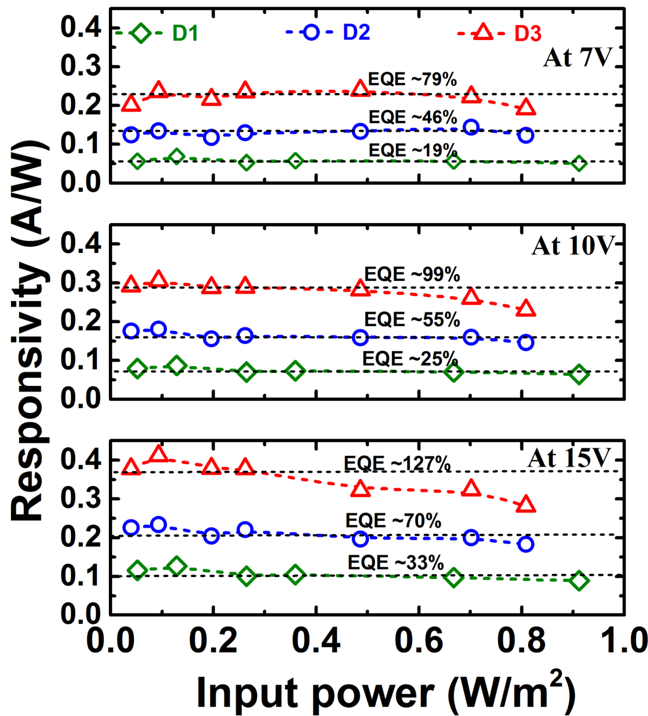

Figure 7. Responsivity and *EQE* of MSM devices D1, D2 and D3 as a function of input power at an incident wavelength of 362 nm and the applied biases of 7, 10 and 15 V.

$\left(\frac{R_{362\ \text{nm}}}{R_{400\ \text{nm}}}\right)$ of 181, 172 and 158 were observed for devices D1, D2 and D3, respectively.

Figure 7 shows the responsivity of MSM devices as a function of input power at an incident wavelength of 362 nm and at the applied biases of 7, 10 and 15 V. All individual devices showed an increase in responsivity with an increase of applied bias. Moreover, at each applied bias, the responsivity of MSM devices was found to be in the order of D1 < D2 < D3, which indicates that the responsivity increases with the decrease of the interdigitated finger spacing, '*S*'. Hence, from these observations, it can be noted that the responsivity increases with the increase of applied electric field between two interdigitated fingers. Further, the observation of *EQE* of >100% indicates the presence of some gain in the sample.

The responsivity is found to be almost flat as a function of input power for the MSM device D1 at all the applied biases, indicating good linearity of this device. The *EQE* of this device varied from 19 to 33% when the applied bias was changed from 7 to 15 V. The MSM device, D2, showed almost flat responsivity with the *EQE* of 46 and 55% at the applied biases of 7 and 10 V, respectively. Some deviation from the flatness of responsivity, indicating non-linearity, has been observed at a higher bias of 15 V and input power of 0.8 W m^{-2}. However, in the case of the MSM device, D3, non-linearity is observed even at a lower bias of 7 V. Moreover, the position of deviation from flatness is observed to shift to lower powers with the increase of the applied bias.

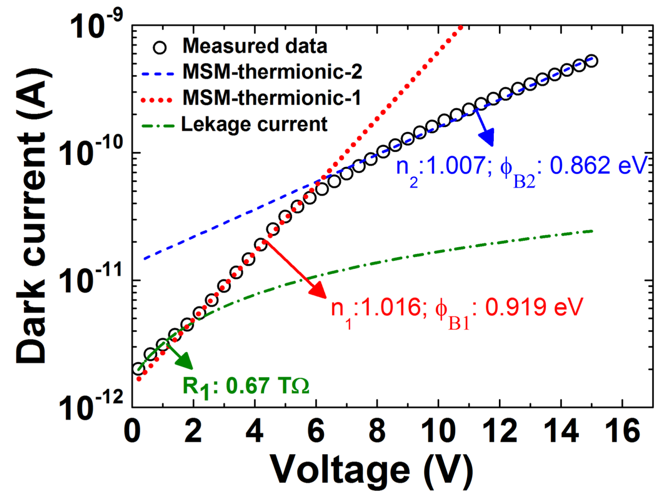

Figure 8. Semi-log plot of dark current and its corresponding fit with the Schottky current transport equation.

Hence, the non-linearity appears to increase with the increase of the electric field between two interdigitated fingers.

The increase in responsivity as a function of electric field between two interdigitated fingers can be attributed to the increased collection efficiency of photo-generated carriers as well as gain due to image force reduction [14] in the devices. In order to investigate the effect of image force reduction in the MSM devices, the dark current measurements were analysed using the equation for the current voltage (*I–V*) characteristics of a Schottky junction [35]

$$I = I_0 \exp\left(\frac{\mathrm{eV}}{nkT}\right)\left[1 - \exp\left(\frac{-\mathrm{eV}}{kT}\right)\right] \tag{6}$$

$$\text{where, } I_0 = AA^*T^2 \exp\left(\frac{-e\phi_B}{nkT}\right)$$

Here, A, A^*, T, V, ϕ_B and n are area, Richardson constant, temperature, applied bias, Schottky barrier height and ideality factor, respectively.

From equation (6), it can be noticed that at an ideality factor of 1 ($n = 1$), the equation becomes a simple form of an ideal Schottky diode equation with the current flow governed only by thermionic emission. However, a deviation in the ideality factor from 1 indicates that the effects, such as image force reduction [14], leakage current [36] and tunneling [35] also play a role in the current characteristics.

Figure 8 shows a typical semi-log plot of dark current and its corresponding fit with equation (1) for device D3 as a function of applied bias beyond 2 V. The *I–V* characteristics follow a linear nature up to 2 V, indicating that the leakage current dominates the current transport mechanism [36]. For applied bias beyond 2 V, an entire *I–V* characteristic curve cannot be fit with a single fitting of equation (1), which shows that the ideality factor as well as barrier height changes as a function of applied bias. Table 1 lists the variation in the ideality factor and the average barrier height with applied bias ranging from 2 to 15 V.

As listed in table 1, the ideality factor is closer to unity with an increase of the applied bias, indicating that the current

Table 1. Variation of the ideality factor and Schottky barrier height in devices D1, D2 and D3 with applied bias.

Device	Ideality factor variation from 2 to 15 V	Schottky barrier height variation from 2 to 15 V (eV)	Net change in Schottky barrier height (eV)
D1	1.008–1.005	0.948–0.931	0.017
D2	1.011–1.007	0.902–0.870	0.032
D3	1.016–1.007	0.919–0.862	0.057

transport mechanism is dominated by thermionic emission. The reduction of the average Schottky barrier height with the applied bias indicates the presence of image force lowering [14] in all the MSM devices. Moreover, the reduction of the barrier height was found to follow in the order D3 > D2 > D1. Hence, with the decrease in '*S*', the electric field between the fingers increases and results in more drop in the barrier height due to image force lowering. Thus, along with the improved collection efficiency for the devices with lower '*S*', the image force lowering also introduces gain in the device to increase the photocurrent as well as the responsivity.

The increase in photocurrent in devices with lower '*S*' might also play a role in the observed drop in responsivity as a function of input power. Similar to the observations in this report, Monroy *et al* [4] have observed a drop in responsivity for GaN-based photoconductors. Based on the model proposed by Garrido *et al* [17], they have attributed the drop to the modulation of conductance by the depleted regions formed around the charged dislocations. Even though the studied samples D1, D2 and D3 are Schottky-based MSM devices, with a carrier concentration of 5.46×10^{15} cm^{-3}, the undepleted portion of the semiconductor occupies a major volume between the two depleted regions under the metal contacts. Further, with a high edge type dislocation density of 5.44×10^{10} cm^{-2}, as estimated from the rocking curve of the GaN $(30\bar{3}2)$ plane, the probability of electrons getting trapped at these dislocations increases. In the case of device D1 with larger interdigitated spacing '*S*' of 9.0 μm, due to the lower collection efficiency as well as lower image force reduction, less photo current passes through the undepleted portion. Hence, even at higher incident power, relatively fewer electrons might have trapped in dislocations, resulting in lower depletion regions around them. If the depleted volume due to the dislocations is negligibly small compared to the undepleted volume, its effect on photo responsivity is negligible and hence the observed flat responsivity for device D1, as shown in figure 7.

In the case of device D2, a similar mechanism can be attributed to the observed flat responsivity at applied biases of 7 and 10 V. However, at an applied bias of 15 V and at higher input power, due to the image force reduction, a larger number of photo-generated electrons pass through the undepleted part and hence are trapped at the dislocations. This has resulted in a significant change in the depleted volume and hence the drop in responsivity. For device D3, a high charge collection efficiency and image force reduction might have caused the drop in responsivity even at the relatively lower applied bias of 7 V as shown in figure 7. When the bias is increased to 10 and 15 V, the photo-generated carriers as well as the trapped electrons at the dislocations further increase due to image force reduction. This results in the dropping of responsivity from flatness even at lower input powers. Hence, the fall of responsivity as a function of input power at higher applied bias and for devices with smaller interdigitated spacing can be attributed to the trapping of electrons in the dislocations.

Thus, overall, GaN MSM Schottky-based photodetectors on Si (111) substrate have been successfully demonstrated with good responsivity to the UV region and sharp cut-off to the visible region using an ammonia-MBE growth technique. When compared to similar devices grown using ammonia-MBE [37], the obtained lower gain for the devices in this study suggests the possibility of improvement in the bandwidth of the device operation. The non-linear nature of the devices due to a responsivity drop with applied input power has not been reported for MSM Schottky-based devices and this effect was only reported on photoconductor-based devices [4]. From this work, it was identified that the similar mechanism that is responsible for non-linearity in photoconductors [17] (conductance modulation due to electron trapping at dislocations) is also responsible for nonlinearity in MSM Schottky-based devices. Furthermore, the dislocation density as well as applied electric filed (i.e. both finger spacing and applied bias) were found to play a major role in determining the linear/nonlinear nature of the MSM Schottky devices. For a fixed grown material with certain dislocation density, by the proper selection of the device dimensions and applied bias, devices with good linearity can be selected for operation.

4. Conclusion

GaN Schottky MSM photodetectors fabricated on Si (111) substrate using the ammonia-MBE growth technique resulted in peak responsivities of 0.071, 0.183 and 0.282 A W^{-1} for devices with finger width '*W*' (μm) and spacing '*S*' (μm) of W6.5S9.0, W4.5S4.5 and W3.0S3.0, respectively. MSM devices exhibited good linearity and flat responsivity characteristics as a function of input power for lower applied electric fields between two interdigitated fingers. However, with the increase of the electric field, the devices showed nonlinearity with a drop in responsivity from flatness as a function of input power. The non-linearity was attributed to the modulation of conductance due to the charging of the dislocations between two successive interdigitated contacts. With the higher electric field, particularly for the devices with lower '*S*', the photocurrent increases due to image force

reduction as well as higher collection efficiency. The higher photocurrent tends to charge the dislocations further by trapping more electrons, resulting in the increased modulation of conductance and drop in responsivity. Hence, the dislocation density and the applied electric field between the fingers were found to control the linearity of GaN MSM devices.

Acknowledgments

The authors would like to acknowledge the funding support from NTU-A*STAR Silicon Technologies Centre of Excellence under the program grant No. 11235100003.

References

[1] Müller A, Konstantinidis G, Androulidaki M, Dinescu A, Stefanescu A, Cismaru A, Neculoiu D, Pavelescu E and Stavrinidis A 2012 Front and backside-illuminated GaN/Si based metal–semiconductor–metal ultraviolet photodetectors manufactured using micromachining and nano-lithographic technologies *Thin Solid Films* **520** 2158–61

[2] Chuang R W, Chang S P, Chang S J, Chiou Y Z, Lu C Y, Lin T K, Lin Y C, Kuo C F and Chang H M 2007 Gallium nitride metal-semiconductor-metal photodetectors prepared on silicon substrates *J. Appl. Phys.* **102** 073110

[3] Khan M A, Kuznia J N, Olson D T, Van Hove J M, Blasingame M and Reitz L F 1992 High-responsivity photoconductive ultraviolet sensors based on insulating single-crystal GaN epilayers *Appl. Phys. Lett.* **60** 2917–9

[4] Monroy E, Calle F, Muñoz E, Omnès F, Beaumont B and Gibart P 1999 Visible-blindness in photoconductive and photovoltaic AlGaN ultraviolet detectors *J. Electron. Mater.* **28** 240–5

[5] Khan M A, Kuznia J N, Olson D T, Blasingame M and Bhattarai A R 1993 Schottky barrier photodetector based on Mg-doped p-type GaN films *Appl. Phys. Lett.* **63** 2455–6

[6] Chen Q, Yang J W, Osinsky A, Gangopadhyay S, Lim B, Anwar M Z, Asif Khan M, Kuksenkov D and Temkin H 1997 Schottky barrier detectors on GaN for visible–blind ultraviolet detection *Appl. Phys. Lett.* **70** 2277–9

[7] Monroy E, Muñoz E, Sánchez F J, Calle F, Calleja E, Beaumont B, Gibart P, Muñoz J A and Cussó F 1998 High-performance GaN p-n junction photodetectors for solar ultraviolet applications *Semicond. Sci. Technol.* **13** 1042

[8] Kuksenkov D V, Temkin H, Osinsky A, Gaska R and Khan M A 1997 Low-frequency noise and performance of GaN p-n junction photodetectors *Electron Devices Meeting, IEDM '97. Tech. Digest., Int.* pp 759–62

[9] Xu G Y *et al* 1997 High speed, low noise ultraviolet photodetectors based on GaN p-i-n and AlGaN(p)-GaN(i)-GaN(n)structures *Appl. Phys. Lett.* **71** 2154–6

[10] Andres de Luna B, Maria T, Gwenole J, Lorenzo R, François Henri J, Shu-Ting C, Yuan-Ting L, Po-Han T and Li-Wei T 2010 Visible-blind photodetector based on p–i–n junction GaN nanowire ensembles *Nanotechnology* **21** 315201

[11] Monroy E, Palacios T, Hainaut O, Omnès F, Calle F and Hochedez J-F 2002 Assessment of GaN metal–semiconductor–metal photodiodes for high-energy ultraviolet photodetection *Appl. Phys. Lett.* **80** 3198–200

[12] Carrano J C, Li T, Grudowski P A, Eiting C J, Dupuis R D and Campbell J C 1998 Comprehensive characterization of metal–semiconductor–metal ultraviolet photodetectors fabricated on single-crystal GaN *J. Appl. Phys.* **83** 6148–60

[13] Averin S, Sachot R, Hugi J, de Fays M and Ilegems M 1996 Two-dimensional device modeling and analysis of GaInAs metal–semiconductor–metal photodiode structures *J. Appl. Phys.* **80** 1553–8

[14] Burm J and Eastman L F 1996 Low-frequency gain in MSM photodiodes due to charge accumulation and image force lowering *Photon. Technol. Lett.* **8** 113–5

[15] Katz O, Garber V, Meyler B, Bahir G and Salzman J 2001 Gain mechanism in GaN Schottky ultraviolet detectors *Appl. Phys. Lett.* **79** 1417–9

[16] Xie F, Lu H, Xiu X, Chen D, Han P, Zhang R and Zheng Y 2011 Low dark current and internal gain mechanism of GaN MSM photodetectors fabricated on bulk GaN substrate *Solid-State Electron.* **57** 39–42

[17] Garrido J A, Monroy E, Izpura I and Muñoz E 1998 Photoconductive gain modelling of GaN photodetectors *Semicond. Sci. Technol.* **13** 563

[18] Semond F, Lorenzini P, Grandjean N and Massies J 2001 High-electron-mobility AlGaN/GaN heterostructures grown on Si(111) by molecular-beam epitaxy *Appl. Phys. Lett.* **78** 335–7

[19] Ravikiran L, Radhakrishnan K, Dharmarasu N, Agrawal M and Basha S M 2013 Strain states of AlN/GaN-stress mitigating layer and their effect on GaN buffer layer grown by ammonia molecular beam epitaxy on 100 mm Si(111) *J. Appl. Phys.* **114** 123503

[20] Ravikiran L, Radhakrishnan K, Munawar Basha S, Dharmarasu N, Agrawal M, Kumar C M M, Arulkumaran S and Ng G I 2015 Study on GaN buffer leakage current in AlGaN/GaN high electron mobility transistor structures grown by ammonia-molecular beam epitaxy on 100 mm Si(111) *J. Appl. Phys.* **117** 245305

[21] Dharmarasu N, Radhakrishnan K, Agrawal M, Ravikiran L, Arulkumaran S, Lee K E and Ing N G 2012 Demonstration of AlGaN/GaN high-electron-mobility transistors on 100 mm-diameter Si(111) by ammonia molecular beam epitaxy *Appl. Phys. Express* **5** 091003

[22] Dai X, Zhang S, Wang Z, Adamo G, Liu H, Huang Y, Couteau C and Soci C 2014 GaAs/AlGaAs nanowire photodetector *Nano Lett.* **14** 2688–93

[23] Vezian S, Natali F, Semond F and Massies J 2004 From spiral growth to kinetic roughening in molecular-beam epitaxy of GaN(0001) *Phys. Rev.* B **69** 125329

[24] Ravikiran L, Dharmarasu N, Radhakrishnan K, Agrawal M, Yiding L, Arulkumaran S, Vicknesh S and Ng G I 2015 Growth and characterization of AlGaN/GaN/AlGaN double-heterojunction high-electron-mobility transistors on 100 mm Si(111) using ammonia-molecular beam epitaxy *J. Appl. Phys.* **117** 025301

[25] Cantu P, Wu F, Waltereit P, Keller S, Romanov A E, Mishra U K, DenBaars S P and Speck J S 2003 Si doping effect on strain reduction in compressively strained Al 0.49Ga0.51N thin films *Appl. Phys. Lett.* **83** 674–6

[26] Reshchikov M A and Morkoç H 2005 Luminescence properties of defects in GaN *J. Appl. Phys.* **97** 061301

[27] Tripathy S, Chua S J, Chen P and Miao Z L 2002 Micro-Raman investigation of strain in GaN and $Al_xGa_{1-x}N$/GaN heterostructures grown on Si(111) *J. Appl. Phys.* **92** 3503–10

[28] Harima H, Nakashima S I and Uemura T 1995 Raman scattering from anisotropic LO-phonon–plasmon–coupled mode in n-type 4H– and 6H–SiC *J. Appl. Phys.* **78** 1996–2005

[29] Wang D, Tin C-C, Williams J R, Park M, Park Y S, Park C M, Kang T W and Yang W-C 2005 Raman characterization of electronic properties of self-assembled GaN nanorods grown

by plasma-assisted molecular-beam epitaxy *Appl. Phys. Lett.* **87** 242105

[30] Demangeot F, Frandon J, Renucci M A, Meny C, Briot O and Aulombard R L 1997 Interplay of electrons and phonons in heavily doped GaN epilayers *J. Appl. Phys.* **82** 1305–9

[31] Wang R X *et al* 2005 Micro-Raman and photoluminescence studies of neutron-irradiated gallium nitride epilayers *Appl. Phys. Lett.* **87** 031906

[32] Barker A S Jr and Ilegems M 1973 Infrared lattice vibrations and free-electron dispersion in GaN *Phys. Rev.* B **7** 743–50

[33] Elhadidy H, Sikula J and Franc J 2012 Symmetrical current–voltage characteristic of a metal–semiconductor–metal structure of Schottky contacts and parameter retrieval of a CdTe structure *Semicond. Sci. Technol.* **27** 015006

[34] Corrion A L, Poblenz C, Wu F and Speck J S 2008 Structural and morphological properties of GaN buffer layers grown by ammonia molecular beam epitaxy on SiC substrates for AlGaN/GaN high electron mobility transistors *J. Appl. Phys.* **103** 093529

[35] Rideout V L 1975 A review of the theory and technology for ohmic contacts to group III–V compound semiconductors *Solid-State Electron.* **18** 541–50

[36] Donoval D, Barus M and Zdimal M 1991 Analysis of I–V measurements on PtSi-Si Schottky structures in a wide temperature range *Solid-State Electron.* **34** 1365–73

[37] Wang X, Wang X, Wang B, Xiao H, Liu H, Wang J, Zeng Y and Li J 2007 High responsivity ultraviolet photodetector based on crack-free GaN on Si (111) *Phys. Status Solidi (*C) **4** 1613–6